

A Subsidence Monitoring Project using a Polarimetric GB-SAR Sensor

Luca Pipia, Xavier Fabregas, Albert Aguasca, Carlos Lopez-Martinez, Jordi. J. Mallorqui, Oscar Mora⁽¹⁾

Universitat Politècnica de Catalunya (UPC),

D3-Campus Nord-UPC, C/ Jordi Girona 1-3, 08034 Barcelona, Spain

{luca.pipia, aguasca, fabregas, carlos.lopez, mallorqui}@tsc.upc.edu

⁽¹⁾Institut Cartogràfic de Catalunya (ICC)

Parc de Montjuïc, 08036, Barcelona, Spain

Abstract – In this paper, the subsidence monitoring activity that the Remote Sensing Laboratory (RSLab) of the Technical University of Catalonia is carrying out in the village of Sallent in the center of Catalonia (Spain) is presented. Polarimetric data have been monthly acquired since June 2006 using a ground-based SAR sensor at X-Band. A detailed description of the deformation phenomenon and of the on-going polarimetric measuring campaign is here given. Finally, first results of polarimetric analysis are discussed.

1. Introduction

The Conca Potàssica Catalana (The Catalan potassic salt basin) is located in the so called Central Catalan Depression, within the Ebre River Depression in the North East of Spain. This basin is made of a great saline unit. The potash salts were traditionally exploited since ancient times, being still an important mining activity in Catalonia. The Enrique mine, located in the city of Sallent, was under exploitation until 1974. This mine had a maximum depth of 260 metres and in 1954 a cavity of approx 120 meters high and 40 meters wide was found while mining works were being done. This cavity, caused by water circulation, is located under the South-East part of Sallent, in the neighbourhood known as Barri de l'Estació, close to the Llobregat River. Water floods in 1957 and 1962 forced to abandon this part of the mine, filling up the cavity with saturated salty water. During the 90s the strong subsidence caused damages in the structures of most of the buildings and some of them had to be demolished. The rest are still under continuous observation (Fig.1). The Catalan Administration started an investigation to identify, quantify and model the subsidence phenomena in this area [1]. Within this program a multiple set of techniques has been applied: topographic leveling, geological mapping, geophysical prospection, extensometric measurements, drilling, orbital DInSAR, etc. in order to evaluate the risk of collapse. In 2003 the SAR group of the UPC, jointly with the ICC, started studying the geological behavior of the district applying DInSAR techniques to ERS1/2 acquisitions. A new collaboration between both two institutions, started at the end of June 2006, is attempting to improve both the spatial accuracy and temporal sampling of the deformation in this area using the innovative ground-based PolInSAR (GB-SAR) system developed at UPC [2].

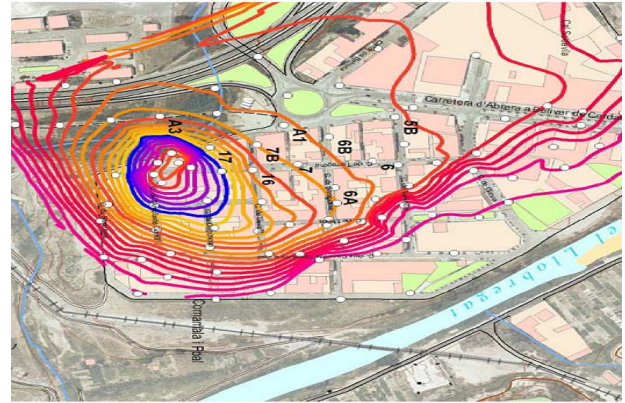


Fig.1: Subsidence Phenomenon in Sallent Village



Fig.2: Photo of Barri de l'Estació from GB-SAR position

2. Experiment Description

When a ground-based SAR solution is adopted for a monitoring activity of phenomenon, the most critical issue is the sensor location: the higher the observation angle with respect to the horizontal plane, the higher the opportunity to reduce the shadowing effects caused by the closer targets. The top of the cliff at the east side of the Llobregat river was selected for this purpose: it is situated at 84 m above the village main plane and about 300 m far from the area of interest. The observation geometry is sketched in Fig.3. The steep slope of the chosen hill allows to avoid any saturation of the radar front-end high-reflectivity close targets might cause. In order to solve zero-baseline errors and to guarantee the placement of the linear unit exactly at the same position, a cement basement with an iron screws grid was realized.

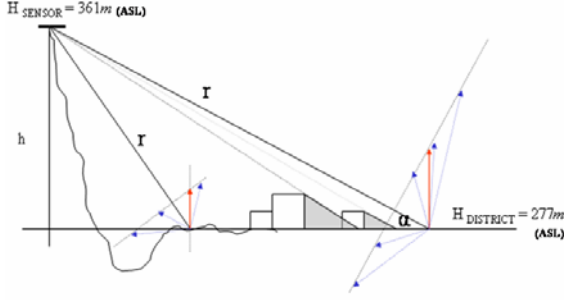


Fig.3: GBSAR acquisition geometry.

A collection of Polarimetric data has been monthly acquired from June to December 2006. The district was observed for approximately 7 hours each day of measure and a time delay of 20 minutes was chosen between successive scans. The main parameters of the measuring campaign are summed up in the Table1. The polarimetric span concerning the area to be monitored is displayed in Fig. 4. The regular structures of the urban environment are easy detectable, as well as the effect of the antennas illumination cone. The darker zones within the image are due to the shadowing effects emphasized in Fig.3 that mainly affect the waste ground areas masked by the closer houses.

3. Polarimetric Calibration

Owing to the absence of extended homogenous areas within the scenario, statistical [3] and iterative [4] techniques for the polarimetric calibration of the data could be applied. An alternative solution, based on the use of passive calibrators was hence used for the purpose. The general formulation of the linear equation system describing the distortion matrix affected a polarimetric measure is [3]:

$$[M] = \begin{bmatrix} R_{hh} & R_{hv} \\ R_{vh} & R_{vv} \end{bmatrix} \begin{bmatrix} S_{hh} & S_{hv} \\ S_{vh} & S_{vv} \end{bmatrix} \begin{bmatrix} T_{hh} & T_{hv} \\ T_{vh} & T_{vv} \end{bmatrix} + N \quad (1)$$

T an R terms represent the elements of the transmission and reception distortion matrices, N takes into account the additive noise. The analysis of a trihedral response placed in the bared area closer to the sensor shows a polarization purity of around 30 dB between the co-polar and cross-polar channels (fig.5). All the products in (1) containing a cross-polar distortion term can be hence neglected (the terms u, v, w, z in [3] are null) and the distortion matrix, diagonal by consequence, leads to a simplified linear equations system:

$$\begin{aligned} M_{hh} &= Y\alpha k^2 S_{hh} \\ M_{hv} &= Yk S_{hv} \\ M_{vh} &= Y\alpha k S_{vh} \\ M_{vv} &= YS_{vv} \end{aligned} \quad (2)$$

where $Yk = \begin{bmatrix} R_{hh} & R_{hv} \\ R_{vh} & R_{vv} \end{bmatrix}$ and $\alpha = \frac{R_{vv} T_{hh}}{T_{vv} R_{hh}}$.

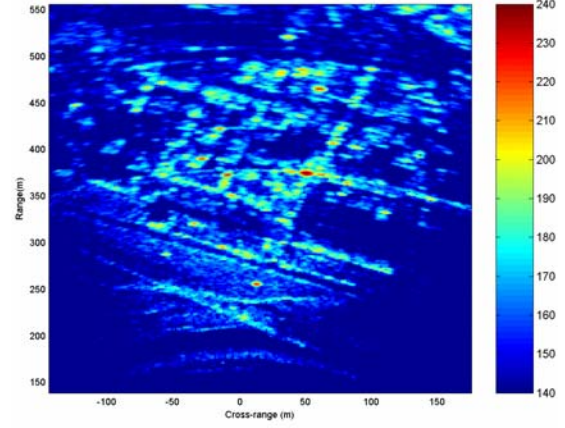


Fig.4: Zoomed Span Image of Estació district measured by the UPC GB Sensor

UPC GB-SAR SYSTEM	
f0 (X-band)	9.65 GHz
PRF	20 KHz
Chirp bandwidth	120 MHz
Base-band bandwidth	40 MHz
A/D sampling rate	100 Ms/sec
Transmitted Power	27 dBm
Time AVG	128
3 dB Beamwidth	30°
Azimuth Sampling	1 cm
Aperture Length	2 m
PolSAR (Stop&Go)	2 min 20sec

Table 1: Measurements Parameters

The Y and k parameters can be found using a corner reflector. In order to estimate the term α , a high reflectivity cross-polar target can be used. An active calibrator (PARC) was excluded: its active nature does not fulfill the conditions for the Reciprocity Theorem applicability and the cross-polar channels equality is verified only when orientated at exactly 45° with respect to the line of sight of the target [5]. Neither a dihedral was considered a suitable solution: the size that guarantees an RCS detectable at a range distance of about 300m makes the calibrator extremely directive and difficult to align with the radar. A hybrid solution was hence adopted: the brudrehedral [6] provides the possibility to obtain a pure cross-polar backscattering when orientated at 45° that presents a reflectivity pattern much less directive than a dihedral of the same size. The UPC GRECO (Graphical Electromagnetic Computing) simulator [7] was first used to fix the parameters defining the reflector's dimensions and then physically realized in the Antenna Laboratory of UPC. Its polarimetric response in a cross-range cut using GB PolSAR real data is shown in Fig.6. Summing up, the radiometric calibration is performed using just a corner reflector whereas the cross-talk correction is obtained using a pure cross-polar target (Bruderhedral), like explained in [8].

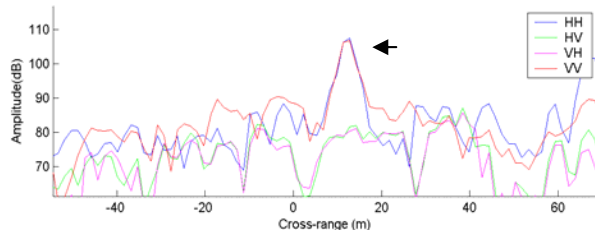


Fig.5: Trihedral response

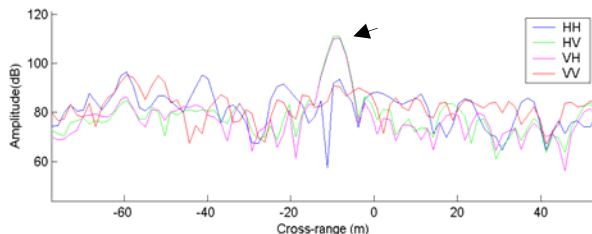
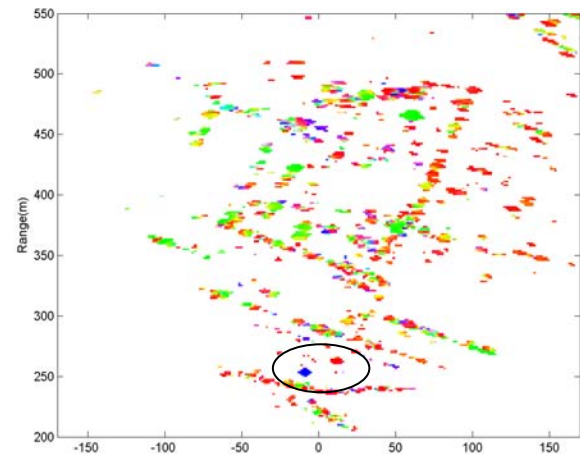


Fig.6: Brudrehedral response

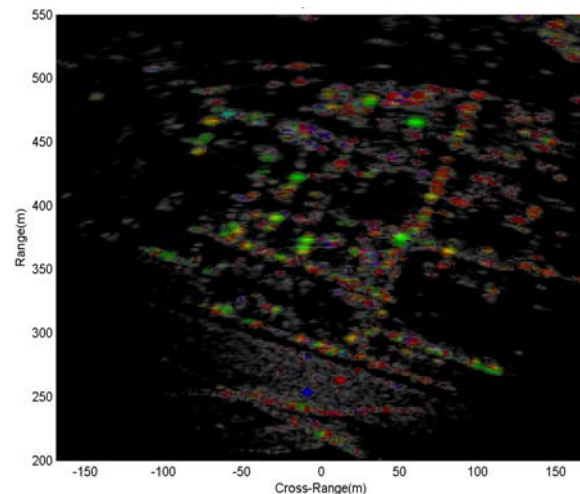
Finally, it must be remarked that a common offset related to the different position of the two calibrators is added to the absolute phase of the four polarimetric channels and introduce an offset that must be compensated for when dealing with multi-temporal zero-baseline acquisitions.

4. Polarimetric Analysis

The deterministic nature of the targets within the urban environment suggests the use of coherent techniques for their polarimetric analysis. The main contribution to the total back-scattered power comes from the co-polar channels, whereas the cross-polar term is generally negligible over the whole image. Only few structures presenting a strong orientation with respect to the radar line of sight can be clearly detected in the HV polarization. This component was explained in terms of multi-path reflections generated by complex deterministic targets more than by pure volumetric scattering. For this reason incoherent techniques will be not taken into consideration in this analysis. The Pauli's Decomposition was applied to the calibrated dataset and the resulting RGB images, both the simple and the weighted by the span, are shown in Fig.7a-b. Their comparison points out the main presence of a dominant scattering mechanism in the most of grid cells within the urban area. Red pixels indicate a single-bounce (trihedral-like) behavior whereas Green for double-bounce (dihedral-like) scattering. Blue points are generated by multiple-reflections phenomena. Yellow pixels, which denote the simultaneous presence of both single and double bounces, are detectable too, although less frequently. Very few cyan and magenta pixels appear. Since the polarimetric information of targets located at the extremes of the antennas illumination cone cannot be trusted, the analysis was limited to the central lobe part. The use of the span parameters to modulate the brightness of the RGB image (Fig 7b) allows to focus the attention on the pixels that are likely to be more stable during one day.



(a) Pauli's RGB Image.



(b) Pauli's RGB Image weighted by span (b)

Figs.7: Pauli's images : Red (Trihedral-like) Green (Dihedral-like) Blue (45°Dihedral-like).

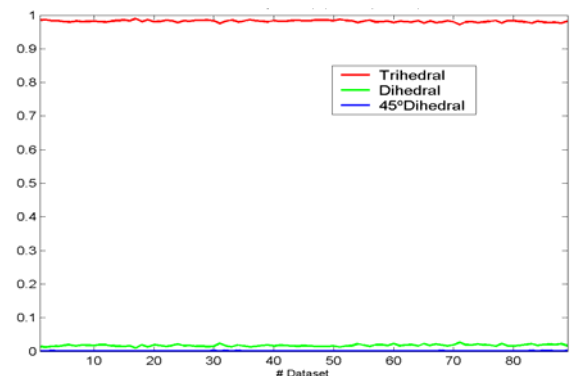


Fig.8: Fixed Trihedral Polarimetric Response.

In the bared area close to ground step, the response of the corner reflector (Red) and the Bruderhedral (Blue) used for calibration are visible within the dark ring. In order to asses the quality of the calibration procedure, in Fig.8 the polarimetric temporal profile of a fixed corner reflector, positioned at approximately 600m from the sensor is shown: the data have been acquired on December 20th/21st, from

MEASUREMENT DAYS						
29/06	26/07	19/09	20/10	14/11	28-9/11	18-9/12
11:00	7:00	10:20	9:00	11:30	17:30	17:00
18:00	13:00	16:30	15:00	17:30	8:30	9:00

Table 2: Days of Measure

6pm am to 6 am. The polarimetric behavior is very pure and stable in the whole temporal sequence. The small fluctuations in the temporal profile are caused by additive noise. On the contrary, the almost negligible dihedral-like contribution is supposed to be generated by the interaction between the reflector and the cement pillar (1×3 meters diameter/height) used as supporting structure.

5. Temporal Analysis

From June to December 2006 polarimetric zero-baseline dataset have been monthly acquired in Sallent (table 2). In order to exploit the set of acquisitions gathered in a whole day of measurements, atmospheric effects had to be first compensated for [9]. The first acquisition was fixed as master and all the successive PolSAR datasets were referred to the master atmospheric conditions, then compensated and finally polimetrically calibrated. Under the hypothesis of stability of deterministic targets response, phase additive noise was reduced applying a time-average to the [S] matrices collection. This procedure was repeated for each day of measure and a collection of 6 days of observation was finally obtained. Since every averaged data was referred to a different atmospheric condition, the measure in June was fixed as reference and the compensation procedure had to be applied again when different months had to be compared. Once estimated, the atmospheric artefact was filtered out from the polarimetric SLC averaged datasets to keep the image maximum resolution. At this point, two different strategies of analysis were possible: a coherence-based or amplitude-based approach. For the coherent technique, a 7×7 averaging windows was used. For the amplitude selection, a simple threshold level was applied to the master data and the obtained mask used for all the slave acquisitions. The differential interferometric phase obtained comparing the time-averaged HH measures of June and October 2006 in two approaches is displayed in Fig.9 and in Fig.10. The result is basically the same although the coherence-based study provides a smoother interferogram and maybe allows to better appreciate the different behavior of the left part of the district with respect to the other half. In the bottom part it can be noticed the deformation of the ground jump (dark ring) related to the erosion effects of rainwater fallen in September. An example of the displacement profile concerning a high-coherent pixel retrieved using the different polarization channels in the coherence approach is also given in Fig.11.

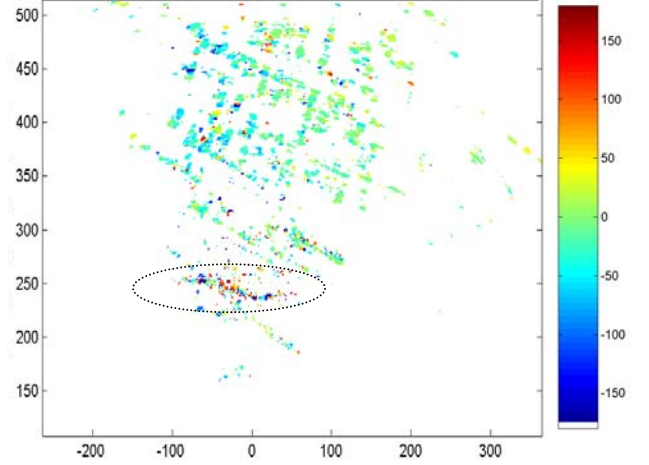


Fig9: Differential Phase (June-October) using Amplitude-Based Approach (HH Polarization)

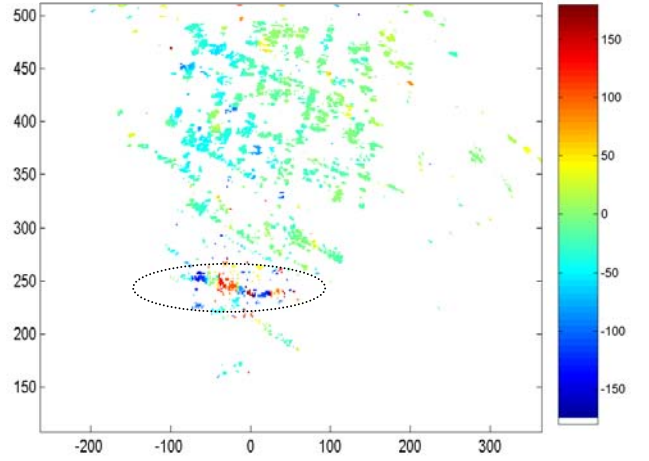


Fig10: Differential Phase (June-October) using Coherence-Based Approach (HH Polarization)

The phase information has been converted in height deformation according to the relation:

$$\Delta r_{vert} = \left(\frac{4\pi}{\lambda} \Delta \phi \right) \frac{R}{h} \quad (3)$$

where R and h are the pixels radial distance and the district main plane height difference from the sensor, respectively. Owing to the short range distance the GB sensor is able to cover, the variations of the incidence angle are significant. The direct consequence is that the same error in the estimation of the radial differential phase is amplified proportionally to R when converted in millimetric vertical displacement (Fig.3). A general overestimation of the deformation has been detected with respect to the velocity of the process during the last years (about 2cm/year in the most critical zone). Unfortunately, the ground-truth measures relative to the monitoring are not available yet. The study that up to this moment has been conducted was based in the analysis of each polarization separately. Since the deformation is supposed to be the same for each

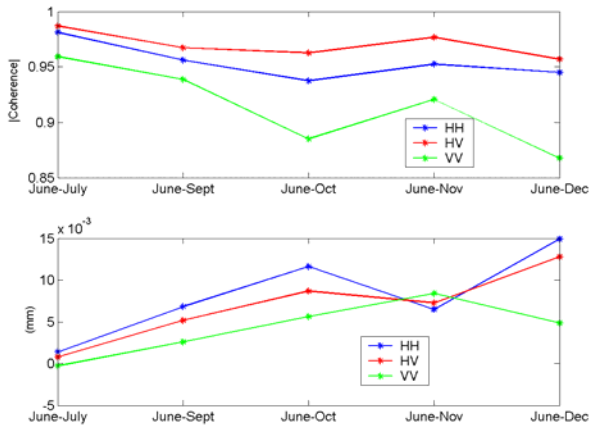


Fig11: Urban Pixel Coherence and vertical displacement profile in the Coherence-Based Approach.

channel of [S], a new approach merging the polarimetric information has to be worked out. Moreover, if the HV term does not seem to be essential for this kind of environment, HH and VV channels are often complementary and would be extremely useful for increasing the search of reliable pixels. The possibility to observe the temporal evolution of urban targets that were supposed to be very stable revealed a dependence of their polarimetric signature on the moment of the day when data are acquired. An example is given in Fig.12, where the profile of the scattering matrix elements concerning a high-reflectivity urban pixel is plotted. About 90 dataset were acquired on December 18th from 5pm to 9am of the next day. The VV amplitude appears more stable than HH, although the power level is approximately the same. Sudden jumps of reflectivity cause important variations in the absolute phase value and are considered responsible for the anomalous behavior of the temporal evolution many high-reflectivity target are subject to. In order to avoid any system failure suspicion, the same temporal profile concerning the corner reflector of fig.8 is displayed in Fig13. The dynamic configuration that an urban area can assume during a whole day directly affects the stability of the target response at X-Band. If a very stable behavior was shown by the pixel selected for the temporal profile of Fig.12 during the night monitoring (18/12/2006), a more instable evolution has been noticed for the same pixel during the day measurements (Fig.14). From this point of view, the dynamic structural properties that an urban environment presents in the diurnal more than in the night hours play a key-role. Moreover, the geometry observation of a ground-based sensor is supposed to increase but not to generate these effects. The choice of the reliable polarimetric description of the targets for long-period observation comparison becomes now critical. A more sophisticated analysis for the most stable daily response must be hence adopted for each pixel in order to improve the retrieval the displacement information.

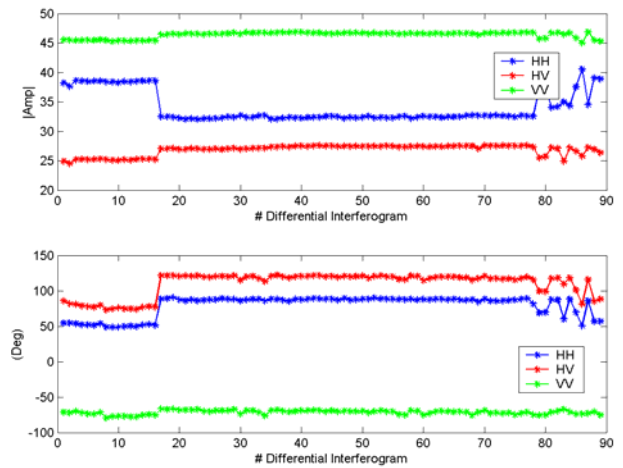


Fig12: Amplitude and Phase temporal evolution of a high reflectivity urban pixel from 5pm on Dec.18th to 9am on Dec.19th.

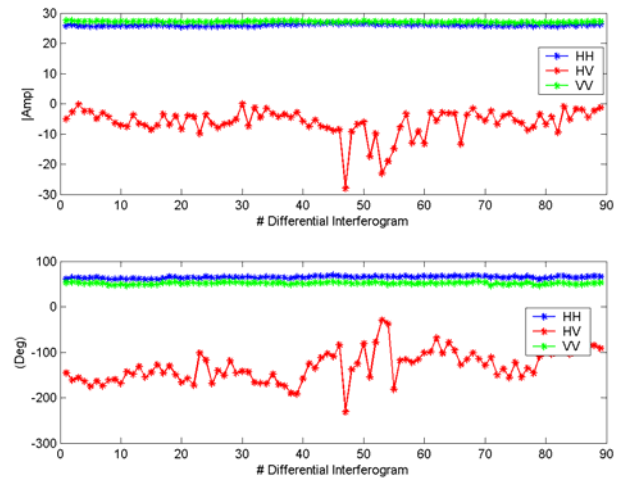


Fig13: Amplitude and Phase temporal evolution of a Trihedral placed at 600m from the sensor from 5pm on Dec.18th to 9am on Dec.19th.

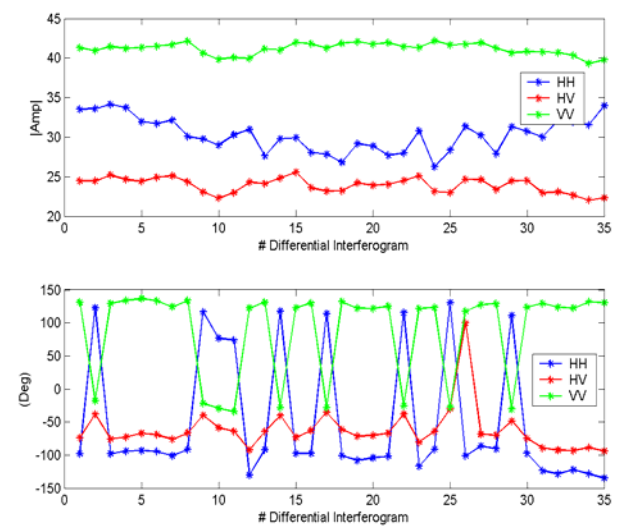


Fig14: Amplitude and Phase temporal evolution of the pixels selected in Fig.14 9am to 15am on Oct.20th.

6. Conclusions

In this paper, the subsidence monitoring activity that the Remote Sensing Laboratory (RSLab) of UPC is carrying out in the village of Sallent using a Polarimetric GB-SAR system has been presented. The observation geometry of the ground-based sensor has been shown to accentuate the shadowing effects, as expected. Nevertheless, the detailed spatial description of the urban environment this solution provides justifies its use for continuous monitoring activity. The possibility to perform a coherence-based and an amplitude-based study of the subsidence phenomenon has been briefly described and first results have been shown.

The study of the polarimetric signature of the urban environment at X-Band has shown that the back-scattered power is mainly contained in the co-polar channels. At the incidence angles defined by the sensor position with respect to the district area, the HH and VV polarizations often provide complementary information that can be merged for improving the stable pixels selection. On the contrary, the cross-polar term does not seem to make an essential contribution to the polarimetric characterization of urban targets, as pointed out by the coherent Pauli's Decomposition.

The study of temporal series of PolSAR data acquired by the ground-based sensor has pointed out the changes in the polarimetric response of pixels within the urban environment. The hypothesis of the signature stability concerning this kind of deterministic targets at X-Band has to be carefully verified before carrying out any results. More sophisticated algorithms for the selection of reliable sequences during the daily acquisitions must be worked out in order to fruitfully study longer temporal evolution of the phenomenon under observation.

Acknowledgements

This work has been funded by the Spanish MCYT under the project TEC 2005-06836-C0201.

References

1. ICC-AR-151-03, 2003. Estudi del process d'esfondrament del terreny que afecta els barris de l'Estació i de la rampinya de Sallent (1997-2003).
2. A. Aguasca, A. Broquetas, J. Mallorquí, X. Fabregas, "A Solid State L to X-band Flexible Ground-Based SAR System for Continuous Monitoring Applications", IGARSS 2004, Anchorage, Alaska.
3. S. Quegan, "A Unified Algorithm for Phase and Cross-Talk Calibration of Polarimetric DATA – Theory and Observations," IEEE TGRS, Vol.32, No.1, January 1994.
4. T. Ainsworth, et al., "Orientation Angle Preserving A Posteriori Polarimetric SAR Calibration," IEEE TGRS, Vol.44, No.4, April 2006.
5. A. Freeman, "SAR Calibration: An Overview" IEEE TGRS, Vol.30, No.6, November 1992.
6. J.D.Silverstein, "Measurements and Predictions of the RCS of Brudherhedrals at Millimetric Wavelength", IEEE TAP, Vol.45, No.7, July 1997.
7. G.Margarit, et al., "On the Usage of GRECOSAR, an Orbital Polarimetric SAR Simulator of Complex Targets, for Vessel Classification Studies, IEEE TGRS, Vol. 44, No 12, December 2006.
8. F.T.Ulaby, C.Elachi, "Radar Polarimetry for Geoscience Applications", Artech House Inc., 1990.
9. L.Pipia et al., "Atmospheric Artifact Estimation and Compensation in Differential Polarimetric GB-SAR Acquisitions," EUSAR2006, Dresde, Germany